

Kinematic and Dynamic Vortices in a Thin Film Driven by an Applied Current and Magnetic Field

Lydia Peres Hari^{*1}, Jacob Rubinstein^{†1}, and Peter Sternberg^{‡2}

¹*Department of Mathematics, Israel Institute of Technology, Haifa 32000, Israel*

²*Department of Mathematics, Indiana University, Bloomington, IN 47405*

January 17, 2013

Abstract

Using a Ginzburg-Landau model, we study the vortex behavior of a rectangular thin film superconductor subjected to an applied current fed into a portion of the sides and an applied magnetic field directed orthogonal to the film. Through a center manifold reduction we develop a rigorous bifurcation theory for the appearance of periodic solutions in certain parameter regimes near the normal state. The leading order dynamics yield in particular a motion law for kinematic vortices moving up and down the center line of the sample. We also present computations that reveal the co-existence and periodic evolution of kinematic and magnetic vortices.

Keywords: Ginzburg-Landau, electric current, magnetic field, kinematic vortex

1 Introduction

We consider a thin superconducting sample occupying a rectangle. The sample is subjected to normal electric current that enters through a lead on one side and leaves through another lead at the opposite side. In addition the sample is subjected to a magnetic field oriented in the direction perpendicular to the rectangle's plane. Our main interest is in the regime in the parameter space where different physical quantities, such as the total current in the sample and the order parameter, are time-periodic. We pay special attention to the formation and motion of vortices in the sample.

The problem above is a natural generalization of the simpler case of a finite superconducting one-dimensional wire subjected to normal current that is fed into one of its endpoints. This problem received considerable attention since it is a canonical case of co-existence of normal current and superconducting current. Moreover, it is known that

^{*}lydia@fermat.technion.ac.il

[†]koby@techunix.technion.ac.il

[‡]Corresponding author, sternber@indiana.edu

in this setting there exists a regime of prescribed current I and temperature T , where the sample's behavior is time-periodic. In addition, in this regime the superconducting order parameter $\psi(x, t)$ vanishes at the wire's center at specific points in time that are separated by a fixed period. Such zeros of ψ are called phase slip centers (PSC). These phenomena and others are studied, numerically and experimentally, by a number of authors including [13, 14, 15], and many of the results are summarized by Ivlev and Kopnin [12].

A recent study in [21] and [22] presents a comprehensive theory that explains the different patterns observed in this wire setting. The key idea is that the underlying system of equations enjoys a PT symmetry, that is, symmetry under complex conjugation and the transformation $x \rightarrow -x$. This symmetry enabled the authors to perform a rigorous bifurcation study of the problem, and to deduce that, under certain conditions, the order parameter bifurcates, as the temperature is lowered beyond a critical value, from the normal state $\psi \equiv 0$ to a nontrivial state. Moreover, this bifurcation is shown to be of Hopf type, and this explains the periodic nature of the solution and the periodic appearance of isolated zeros of ψ .

In the present study we look at a more realistic geometry of a finite strip. Moreover, we consider not just forced electric current, but also the effect of an external magnetic field. The problem is analyzed numerically in [6]. The authors observe, just as in the one-dimensional setting, a periodic behavior of a number of physical quantities, including periodic appearance and motion of vortices. Therefore, our goal is to derive a theory that explains the observed patterns and vortex motion.

The issue of vortices is of particular interest. They are defined as isolated zeros of the order parameter, and they are characterized by their topological degree in the (x, y) plane. The appearance of vortices in superconducting samples subjected to an applied magnetic field is of course well-known. Therefore, we expect them in our setting even in the absence of forced electric currents. What makes the present problem interesting is that also the opposite is true; namely, vortices form, for appropriate range of values of I and T , even if no magnetic field is applied. Therefore, one can classify the vortices here into magnetic vortices generated by the applied magnetic field in the absence of any applied current, and kinematic vortices generated, as will be shown below, by the forced electric field and the special symmetry of the problem in the absence of any magnetic field.

When both applied magnetic and electric fields are present, it is not as clear how to make a distinction between the two kinds of vortices. As will be shown below, the symmetry of the problem implies that some vortices are formed and move time-periodically on the center line of the rectangle for large enough I and for a range of applied magnetic fields h . We term them kinematic vortices. In certain cases, as presented below, these kinematic vortices collide and move off the center line. We term such vortices, “born” from kinematic vortices, ‘kinematic’ as well.

Other vortex phenomena, not usually observed in more standard Ginzburg-Landau settings, include the time-periodic emergence of vortex pairs that are of opposite degrees, which we term vortex/anti-vortex pairs: typically stable vortex configurations of Ginzburg-Landau vortices only involve vortices of the same degree but in this periodic setting that is not always the case. We also show that for some range of I and h vortices of *the same degree* move towards each other and collide before moving away from

each other. Again, this is a process that is atypical to more familiar Ginzburg-Landau settings.

The analysis of the present problem follows to some extent the lines of the one-dimensional wire problem. Namely, we construct a proper framework that enables us to use the Center Manifold Theorem to study the bifurcation picture, and thereby establish the existence of a Hopf bifurcation. Moreover, in both cases a key factor is played by the spectrum of the underlying linear Schrödinger operator. However, there are a few important differences between the one-dimensional case and the problem considered here. First, the construction of the center manifold requires certain apriori estimates on the solutions to the underlying differential equations. These estimates are harder to obtain in the two-dimensional setting. A second important difference relates to the vortex motion. While in the one-dimensional case the PSCs just appear momentarily at a fixed periodic sequence of instances, the kinematic vortices in the two-dimensional problem are present for periodic finite time intervals. Moreover, they tend to move along or near the y -axis (which is the center line of the rectangle) as we shall show.

It is interesting to note that implications of PT-symmetry seem to appear in a number of quite different physical problems. For instance, we mention applications to quantum mechanics [4], [8], to hydrodynamic instability [24], [25], and to optics [19], [20]. We also mention several recent rigorous studies within Ginzburg-Landau theory that incorporate magnetic effects along with applied currents in a variety of asymptotic regimes, [1, 2, 9, 23, 26]. One aspect of our investigation that distinguishes it from others, however, is that it is to our knowledge the first to capture a motion law for Ginzburg-Landau vortices that is not based on the assumption of large Ginzburg-Landau parameter.

In the next section we formulate the problem and the underlying equations. The bifurcation analysis is performed in section 3. In particular we establish there the existence of a center manifold for a certain regime in the (I, T) plane. In section 4 we consider the formation of vortices and their motion and discuss some computational work on the problem.

2 Formulation of Problem

We consider a superconducting material occupying a thin rectangular box with dimensions $-L < x < L$, $-K < y < K$ and say $0 < z < \eta$ where η is assumed to be much smaller than the coherence length or penetration depth, allowing us to work within the thin film 2d approximation of Ginzburg-Landau. In this approximation, we take the complex-valued order parameter $\Psi = \Psi(x, y, t)$ and the real-valued electric potential $\phi = \phi(x, y, t)$ to be defined on $\mathcal{R} \times [0, \infty)$ where we denote $\mathcal{R} := [-L, L] \times [-K, K]$ and we ignore any induced magnetic field. Within this rectangular geometry, we assume the presence of leads forcing in electric current of magnitude I through the sides $x = \pm L$, along the subinterval $-\delta < y < \delta$ for some positive $\delta < K$. Additionally we assume that the thin film is subjected to an applied magnetic field of size h oriented perpendicular to the rectangular cross-section. See Figure 1.

Introducing the applied magnetic potential $A_0 := (-y, 0)$, this applied field is then given by $h\nabla \times A_0$ and the thin film limit of Ginzburg-Landau takes the nondimension-

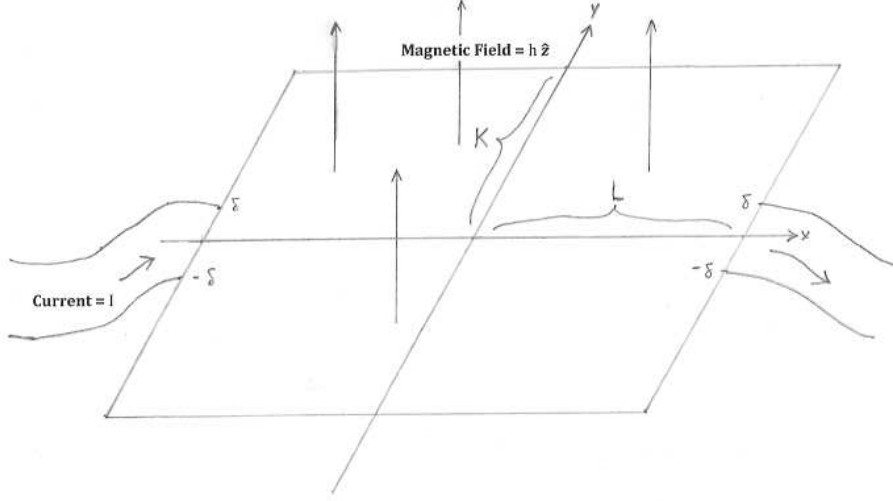


Figure 1: A thin film superconductor subjected to applied current and magnetic field.

alized form

$$\Psi_t + i\phi\Psi = (\nabla - ihA_0)^2\Psi + (\Gamma - |\Psi|^2)\Psi \quad \text{for } (x, y) \in \mathcal{R}, t > 0, \quad (2.1)$$

$$\Delta\phi = \nabla \cdot \left(\frac{i}{2} \{ \Psi \nabla \Psi^* - \Psi^* \nabla \Psi \} - |\Psi|^2 h A_0 \right) \quad \text{for } (x, y) \in \mathcal{R}, t > 0, \quad (2.2)$$

subject to the boundary conditions

$$\Psi(\pm L, y, t) = 0 \quad \text{for } |y| < \delta, \quad (2.3)$$

$$\Psi_x(\pm L, y, t) + ihy\Psi(\pm L, y, t) = 0 \quad \text{for } \delta < |y| \leq K, \quad (2.4)$$

$$\Psi_y(x, \pm K, t) = 0 \quad \text{for } |x| \leq L, \quad (2.5)$$

$$\phi_x(\pm L, y, t) = \begin{cases} -I & \text{for } |y| < \delta, \\ 0 & \text{for } \delta < |y| < K \end{cases} \quad (2.6)$$

$$\phi_y(x, \pm K, t) = 0 \quad \text{for } |x| \leq L. \quad (2.7)$$

along with the initial condition $\Psi(x, y, 0) = \Psi_{init}(x, y)$. As a convenient normalization we take $\int_{\mathcal{R}} \phi = 0$. The system of equations above are collectively known as the Time-Dependent Ginzburg-Landau (TDGL) model.

The parameter Γ is proportional to $T - T_c$ where T is temperature and T_c is the critical temperature below which the normal (zero) state loses stability in the absence of any applied fields. Note that (2.2) is simply the requirement of conservation of total (normal + superconducting) current. Also, we remark that the boundary conditions (2.4)-(2.5) are the standard superconductor/vacuum conditions on Ψ , while (2.3) reflects the presence of the normal leads.

There are numerous investigations of current-driven superconducting wires and thin films that utilize a model based on Ginzburg-Landau theory, and these have generally reported reasonable agreement between theory and experiment. Regarding (2.1), we should mention that some studies on this problem such as [5, 6, 18] replace the left-hand side with the modification

$$\frac{u}{\sqrt{1 + \gamma^2 |\Psi|^2}} \left(\frac{\partial}{\partial t} + i\phi + \frac{\gamma^2}{2} \frac{\partial |\Psi|^2}{\partial t} \right) \Psi,$$

where u and γ are material parameters. However, we believe that the standard and simpler evolution equation (2.1) corresponding to the choices $u = 1$ and $\gamma = 0$ captures the main features of the problem, an opinion shared by the authors of [3] whose computational comparisons suggest that the modification does not have a large effect in this setting. What is more, in what follows, we shall concentrate on bifurcation from the normal state $\Psi \equiv 0$, so the smallness of the amplitude should mute the effect of this modification even more.

3 Analysis of the model

For a given Ψ , and a given value $h \geq 0$, let us decompose the solution ϕ to (2.2), (2.6), (2.7) as

$$\phi = I\phi^0 + \tilde{\phi}$$

and where ϕ^0 is harmonic and satisfies the boundary conditions

$$\phi_x^0(\pm L, y) = \begin{cases} -1 & \text{for } |y| < \delta, \\ 0 & \text{for } \delta < |y| < K, \end{cases} \quad (3.1)$$

$$\phi_y^0(x, \pm K) = 0 \text{ for } |x| \leq L, \quad (3.2)$$

while $\tilde{\phi}$ satisfies (2.2) subject to homogeneous Neumann boundary conditions on all portions of the rectangular boundary. We note that $\tilde{\phi}$ but depends on Ψ so we will often write $\tilde{\phi}$ as $\tilde{\phi}[\Psi]$ to emphasize this dependence.

We will occasionally make use of the properties

$$\phi^0(-x, y) = -\phi^0(x, y) \quad \text{and} \quad \phi^0(x, -y) = \phi^0(x, y), \quad (3.3)$$

which are easy to check.

The normal state in this setting corresponds to $\Psi \equiv 0$ and $\phi \equiv I\phi^0$. We will pursue a bifurcation analysis about this normal state, and therefore a crucial role will be played by the linear eigenvalue problem

$$\mathcal{L}[u] := (\nabla - ihA_0)^2 u - iI\phi^0 u = -\lambda u \quad \text{for } |x| < L, |y| < K, \quad (3.4)$$

subject to the boundary conditions (2.3)–(2.5). Though we do not indicate it in our notation, it is understood that \mathcal{L} and therefore all of its eigenvalues and eigenfunctions depend on the parameters L, K, δ, h and I . We summarize below the key properties of the corresponding eigenvalues and eigenfunctions that will be needed in the analysis to follow.

Lemma 3.1. *The spectrum of \mathcal{L} consists only of point spectrum, denoted by $\{\lambda_j\}$ with corresponding eigenfunctions $\{u_j\}$. If (λ_j, u_j) is an eigenpair satisfying (3.4) then*

$$\operatorname{Re} \lambda_j > 0, \quad \text{and} \quad |\operatorname{Im} \lambda_j| < \|\phi^0\|_{L^\infty} I. \quad (3.5)$$

Thus, in particular we may order the eigenvalues $\lambda_1, \lambda_2, \dots$ according to the size of their real part, with $0 < \operatorname{Re} \lambda_1 \leq \operatorname{Re} \lambda_2 \leq \dots$. The PT -symmetry of the operator is reflected in the fact that if (λ_j, u_j) is an eigenpair then so is $(\lambda_j^, u_j^\dagger)$ where $u_j^\dagger(x, y) := u_j^*(-x, y)$.*

When working with u_1 and u_2 , we will choose the normalization

$$\int_{\mathcal{R}} u_1^2 = 1 = \int_{\mathcal{R}} u_2^2. \quad (3.6)$$

Also, as a matter of convention, when λ_1 is non-real, we associate u_1 with the eigenvalue λ_1 having positive imaginary part, and u_2 with λ_1^* .

Proof. The fact that the spectrum consists solely of eigenvalues follows from standard compact operator theory. The conditions in (3.5) follow from multiplication of the equation $\mathcal{L}[u] = -\lambda u$ by u^* and integration over the rectangle. This leads to the identity

$$\lambda = \frac{\int_{\mathcal{R}} |(\nabla \pm i h A_0) u|^2}{\int_{\mathcal{R}} |u|^2} + i I \frac{\int_{\mathcal{R}} \phi^0 |u|^2}{\int_{\mathcal{R}} |u|^2}, \quad (3.7)$$

implying (3.5).

The final claim of the lemma follows by noting that $\mathcal{L}[u^\dagger] = \mathcal{L}[u]$. \square

A numerical analysis of the eigenvalue problem (3.4) indicates that, fixing all other parameters (i.e. K, L, δ and h) and varying only the current I , there exists a critical value I_c depending on these other parameters, such that λ_1 is real for $I \leq I_c$ and λ_1 is non-real for $I > I_c$. This complexification of λ_1 arises through a collision with another eigenvalue and the two eigenvalues emerge from this collision, that is for $I > I_c$, as complex conjugate pairs. Examples of eigenvalue collisions are shown in Figures 2a and 2b. In both cases the simulated geometry is $L = 1, K = 2/3, \delta = 4/15$. In Figure 2a we took $h = 0$, while in Figure 2b we took $h = 7.5$.

We note in passing that in light of (3.3) and (3.7), the evenness of $|u_j|$ evidently implies reality of λ_j so the passage to complex eigenvalues with increased values of I carries with it a certain symmetry breaking of the corresponding eigenfunction. This phenomenon has been established rigorously for the one-dimensional version of (3.4)—that is, for the problem depending only on x and with $h = 0$ in [24, 25]. The reality of the spectrum for I positive and sufficiently small in this two-dimensional setting should follow by the type of perturbation analysis to be found in [7], since for $I = 0$, the spectrum is clearly real, cf. (3.5). However, since here we are interested in the regime where the first eigenvalue is complex, we do not pursue this point further.

Regarding eigenvalue collisions, we also wish to note another new phenomenon for this two-dimensional problem with the incorporation of magnetic effects that is not observed for the one-dimensional problem. Our computations reveal that for certain large enough values of applied magnetic field h , as I increases through the regime $0 < I < I_c$, the

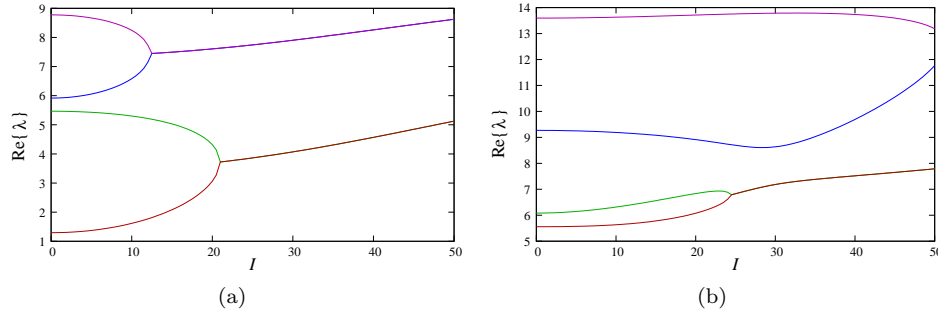


Figure 2: The real part of the spectrum of \mathcal{L} . The first 4 eigenvalues are drawn for the parameters $L = 1, K = 2/3, \delta = 1/6$. In (a) $h = 0$, while in (b) $h = 7.5$

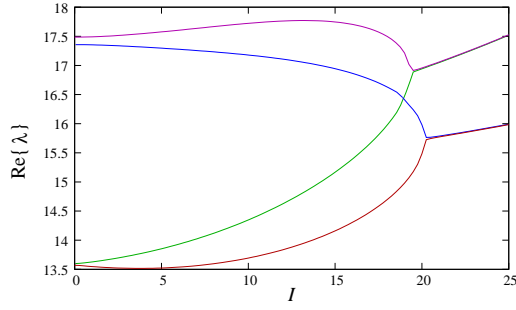


Figure 3: The real parts of the four leading eigenvalues for the parameter values $L = 1, K = 2/3, \delta = 4/15, h = 20, I = 25$. Note how λ_3 passes through λ_2 and then collides with λ_1 at $I = I_c \approx 20$.

second and third (still real) eigenvalues pass through each other and it is ultimately what was originally labeled as the third eigenvalue that collides with λ_1 at I_c . We say the third eigenvalue “passes through” the second rather than “collides” with it because as I varies through the point where $\lambda_2 = \lambda_3$, both eigenvalues remain simple and the corresponding eigenfunctions vary smoothly without incident. This for example is the scenario for the parameter values $L = 1, K = 2/3, \delta = 4/15, h = 20, I = 25$. See Figure 3. We will return to this set of parameter values at the end of the article to discuss anomalous vortex behavior as well.

At this point we fix any values of K, L, δ, h and then pick I sufficiently large so that $\text{Im } \lambda_1 \neq 0$. We then consider our problem (2.1)–(2.7) with Γ given by $\Gamma = \text{Re } \lambda_1 + \varepsilon$ where ε is small and positive. Note that given the temperature dependence of Γ , this corresponds to lowering the temperature just below the value where the normal states becomes linearly unstable.

We now introduce the linear operator $\mathcal{L}_1[u] := \mathcal{L}[u] + (\text{Re } \lambda_1) u$. Recalling Lemma 3.1 in the scenario where λ_1 is not real, the corresponding first eigenfunctions, say u_1 and

u_2 , satisfy

$$u_2 = u_1^\dagger \quad \text{with} \quad \mathcal{L}_1[u_1] = -i \operatorname{Im} \lambda_1 u_1, \quad \mathcal{L}_1[u_2] = i \operatorname{Im} \lambda_1 u_2. \quad (3.8)$$

For later use, we also note that if we introduce the adjoint operator \mathcal{L}_1^* satisfying

$$\int_{\mathcal{R}} \mathcal{L}_1[u]v = \int_{\mathcal{R}} \mathcal{L}_1^*[v]u,$$

then we can readily identify $\mathcal{L}_1^*[v]$ as simply the operator given by $(\nabla + ihA_0)^2 v - iI\phi^0 v + (\operatorname{Re} \lambda_1) v$. Furthermore, the fact that ϕ_0 is even in y (cf. (3.3)) reveals that the functions $u_j^*(x, y) := u_j(x, -y)$ for $j = 1, 2$ satisfy the equations

$$\mathcal{L}_1^*[u_1^*] = -i \operatorname{Im} \lambda_1 u_1^*, \quad \mathcal{L}_1^*[u_2^*] = i \operatorname{Im} \lambda_1 u_2^*.$$

Consequently, we see that

$$-i \operatorname{Im} \lambda_1 \int_{\mathcal{R}} u_1^* u_2 = \int_{\mathcal{R}} \mathcal{L}_1^*[u_1^*] u_2 = \int_{\mathcal{R}} \mathcal{L}_1[u_2] u_1^* = i \operatorname{Im} \lambda_1 \int_{\mathcal{R}} u_1^* u_2,$$

with a similar relation holding between u_2^* and u_1 . Hence, $\int_{\mathcal{R}} u_1^* u_2 = 0 = \int_{\mathcal{R}} u_2^* u_1$. Clearly, this orthogonality holds between any two eigenfunctions u_j and u_k of the operator \mathcal{L}_1 corresponding to distinct eigenvalues, namely

$$\int_{\mathcal{R}} u_j^* u_k = 0 \quad \text{for } j \neq k. \quad (3.9)$$

Of course, in the special case of no applied magnetic field, i.e. $h = 0$, we have $\mathcal{L} = \mathcal{L}^*$ and $u_1 = u_1^*$ and through (3.3) we see then that each eigenfunction is even in y .

Let us now return to the (2.1)-(2.2) with the choice $\Gamma = \operatorname{Re} \lambda_1 + \varepsilon$ and re-express the system as a single nonlinear, non-local equation for the complex-valued order parameter Ψ :

$$\Psi_t = \mathcal{L}_1[\Psi] + \varepsilon \Psi + \mathcal{N}(\Psi), \quad (3.10)$$

where

$$\mathcal{N}(\Psi) := -|\Psi|^2 \Psi - i\tilde{\phi}[\Psi]\Psi. \quad (3.11)$$

When expressed in this form, the problem can be rigorously solved for $\varepsilon \ll 1$ via a center manifold reduction. The analysis is similar to that carried out for the one-dimensional (thin wire) problem in [22], Prop. 6.8, so we will only mention the key steps and those parts of the calculation where there are changes.

As regards the linear part of (3.10), the key point is that the operator $-\mathcal{L}_1$ is sectorial, in light of (3.5), cf. [11]. Regarding estimates on the cubic, nonlocal nonlinearity \mathcal{N} , the analysis differs from that in [22] in that for the one-dimensional problem it is easy to check that \mathcal{N} is a bounded map from H^1 to H^1 (cf. [22], Lemma 6.3), while in the present two-dimensional setting this is no longer true—it just barely misses. One way to overcome this obstacle is by viewing \mathcal{N} as a mapping from an interpolation space between H^1 and H^2 into L^2 . The details of pursuing this strategy can be found in section 3.4 of [17], where the authors execute a center manifold construction relevant to bifurcation

from the normal state without applied electric current. Alternatively, one can view \mathcal{N} as a map from $H^2(\mathcal{R})$ into $H^1(\mathcal{R})$. We describe how to make the necessary estimates for this latter approach.

Writing $\mathcal{N} = \mathcal{N}_1 + \mathcal{N}_2$ with $\mathcal{N}_1(\Psi) := -|\Psi|^2 \Psi$ and $\mathcal{N}_2(\Psi) := -i\tilde{\phi}[\Psi]\Psi$, it is an easy application of Hölder's inequality to make the estimate

$$\|\mathcal{N}_1(\Psi)\|_{H^1(\mathcal{R})} \leq C \|\Psi\|_{H^2(\mathcal{R})}^3. \quad (3.12)$$

To make a similar estimate on \mathcal{N}_2 , let us first write the PDE coming from (2.2) for $\tilde{\phi}(\Psi)$ as

$$\Delta \tilde{\phi} = \nabla \cdot \left(j(\Psi) - |\Psi|^2 A_0 \right), \quad (3.13)$$

subject to homogeneous Neumann conditions and the normalization condition of mean zero, where we have introduced the notation $j(\Psi) := \frac{i}{2} \{ \Psi \nabla \Psi^* - \Psi^* \nabla \Psi \}$. Fixing any $p \in (1, 2)$ we may use Hölder's inequality and Sobolev imbedding to make the estimate

$$\begin{aligned} \int_{\mathcal{R}} |Dj(\Psi)|^p &\leq C \int_{\mathcal{R}} \left(|\Psi|^p |D^2 \Psi|^p + |D\Psi|^{2p} \right) \\ &\leq C \left(\|\Psi\|_{H^2(\mathcal{R})}^p \|\Psi\|_{L^{2p/(2-p)}(\mathcal{R})}^p + \|\Psi\|_{W^{1,2p}(\mathcal{R})}^{2p} \right) \leq C \|\Psi\|_{H^2(\mathcal{R})}^{2p}. \end{aligned}$$

Hence, $\|Dj(\Psi)\|_{L^p(\mathcal{R})} \leq C \|\Psi\|_{H^2(\mathcal{R})}^2$. It is also easy to estimate

$$\|j(\Psi)\|_{L^p(\mathcal{R})} + \left\| |\Psi|^2 A_0 \right\|_{W^{1,p}(\mathcal{R})} \leq C \|\Psi\|_{H^2(\mathcal{R})}^2,$$

so we conclude that

$$\left\| \nabla \cdot (j(\Psi) - |\Psi|^2 A_0) \right\|_{L^p(\mathcal{R})} \leq C \|\Psi\|_{H^2(\mathcal{R})}^2.$$

Then appealing to the Calderon-Zygmund inequality (cf. [27], Chapter 2), equation (3.13) implies that

$$\left\| \tilde{\phi}(\Psi) \right\|_{W^{2,p}(\mathcal{R})} \leq C \|\Psi\|_{H^2(\mathcal{R})}^2.$$

From the Sobolev imbedding theorem and Hölder's inequality it then follows easily that $\|\mathcal{N}_2(\Psi)\|_{H^1(\mathcal{R})} \leq C \|\Psi\|_{H^2(\mathcal{R})}^3$. Combining this last estimate with (3.12) we arrive at the estimate on the nonlinearity:

$$\|\mathcal{N}(\Psi)\|_{H^1(\mathcal{R})} \leq C \|\Psi\|_{H^2(\mathcal{R})}^3. \quad (3.14)$$

The upshot is that for each small ε , one can construct a center manifold \mathcal{M}_ε as a graph $v \mapsto \Phi(v, \varepsilon)$ in $H^2(\mathcal{R})$ over the center subspace $\mathcal{S} := \text{span}\{u_1, u_2\}$, applying for example, the version of the Center Manifold Theorem to be found in [10], Theorem 2.9. More precisely, there exist positive constants δ_0 and ε_0 , such that for any ε satisfying $|\varepsilon| \leq \varepsilon_0$ one can define $\mathcal{M}_\varepsilon := \{\Phi(v, \varepsilon) : v \in \mathcal{S}, \|v\|_{H^2(\mathcal{R})} < \delta_0\}$, and \mathcal{M}_ε enjoys the following properties:

(i) The center manifold is locally invariant for the flow (3.10) in the sense that if $|\varepsilon| < \varepsilon_0$ and the initial data ψ_0 lies on \mathcal{M}_ε , then so does the solution ψ^ε to (3.10) so long as $\|\psi^\varepsilon(\cdot, t)\|_{H^2(\mathcal{R})}$ stays sufficiently small. Hence, for such initial data, one can describe the resulting solution $\psi^\varepsilon(t) = \psi^\varepsilon(\cdot, t)$ through two maps $\alpha_1^\varepsilon, \alpha_2^\varepsilon : [0, \infty) \rightarrow \mathbb{C}$ via $\psi^\varepsilon(t) = \Phi(\alpha_1^\varepsilon(t)u_1 + \alpha_2^\varepsilon(t)u_2, \varepsilon)$. Since u_1 and u_2 are fixed throughout, we will often write simply

$$\psi^\varepsilon(t) = \Phi(\alpha_1^\varepsilon(t), \alpha_2^\varepsilon(t), \varepsilon) \quad (3.15)$$

for the sake of brevity.

(ii) The center manifold is PT-symmetric, i.e. $\psi \in \mathcal{M}_\varepsilon \implies \psi^\dagger \in \mathcal{M}_\varepsilon$. Furthermore, if $v = v^\dagger$, then $\Phi(v, \varepsilon) = \Phi^\dagger(v, \varepsilon)$. Since $u_2 = u_1^\dagger$, this implies that if $\alpha_2^\varepsilon(0) = \alpha_1^\varepsilon(0)^*$, and one solves (3.10) subject to the PT-symmetric initial conditions $\psi^\varepsilon(0) = \Phi(\alpha_1^\varepsilon(0), \alpha_2^\varepsilon(0), \varepsilon)$, then the resulting functions $\alpha_1^\varepsilon(t)$ and $\alpha_2^\varepsilon(t)$ describing the solution ψ^ε at any positive time t will remain complex conjugates.

(iii) \mathcal{M} contains all nearby bounded solutions of (3.10), and in particular, it contains any nearby steady-state or time-periodic solutions.

(iv) Through an appeal to (3.14), the discrepancy between the center manifold and the center subspace can be expressed through the estimate

$$\|\Phi(v, \varepsilon) - v\|_{H^2(\mathcal{R})} \leq C_1 \left(\|v\|_{H^2(\mathcal{R})}^3 + |\varepsilon| \|v\|_{H^2(\mathcal{R})} \right) \quad (3.16)$$

which holds for any pair (v, ε) such that $v \in \mathcal{S}$ with $\|v\|_{H^2(\mathcal{R})} < \delta_0$ and $|\varepsilon| < \varepsilon_0$, where C_1 is a positive constant independent of v and ε .

Armed with these properties of the center manifold, one can then fix any sufficiently small complex numbers $\alpha_1^\varepsilon(0)$ and $\alpha_2^\varepsilon(0)$ as in (i) above, solve (3.10) and then use the projection Π_c onto the center subspace \mathcal{S} to obtain a reduced system of O.D.E.'s governing the evolution of α_1^ε and α_2^ε . In light of (3.9) we can write an arbitrary function f as $f = c_1 u_1 + c_2 u_2 + u^\perp$ where $u^\perp \in (\text{span}\{u_1^*, u_2^*\})^\perp$. Hence the projection onto the center subspace of an arbitrary function f is given by

$$\Pi_c(f) = \left(\frac{\int_{\mathcal{R}} u_1^* f}{\int_{\mathcal{R}} u_1^* u_1} \right) u_1 + \left(\frac{\int_{\mathcal{R}} u_2^* f}{\int_{\mathcal{R}} u_2^* u_2} \right) u_2.$$

Thus, substituting the reduction (3.15) into (3.10) and projecting, we obtain the following system through the use of (3.8):

$$\begin{aligned} \dot{\alpha}_1^\varepsilon u_1 + \dot{\alpha}_2^\varepsilon u_2 &= (\varepsilon - i \text{Im } \lambda_1) \alpha_1^\varepsilon u_1 + (\varepsilon + i \text{Im } \lambda_1) \alpha_2^\varepsilon u_2 \\ &+ \Pi_c \left(\mathcal{N}(\alpha_1^\varepsilon u_1 + \alpha_2^\varepsilon u_2) \right) + \left\{ \Pi_c \left(\mathcal{N}(\Phi(\alpha_1^\varepsilon, \alpha_2^\varepsilon, \varepsilon)) \right) - \Pi_c \left(\mathcal{N}(\alpha_1^\varepsilon u_1 + \alpha_2^\varepsilon u_2) \right) \right\}, \end{aligned} \quad (3.17)$$

where $\dot{\cdot}$ denotes a time derivative.

Invoking (3.16), one finds that the last expression above involving the difference of nonlinear terms is lower order so one is justified in initially ignoring it, solving the

resulting simplified system of O.D.E.'s and then arguing that the behavior of solutions persists for the full system (3.17). Again the details of this portion of the argument can be found in [22]. In an abuse of notation, we will persist in using the notation α_j^ε to denote the solution to the truncated system in which the last expression is dropped.

Now using (3.9), we integrate first against u_1^* and then against u_2^* to arrive at the system:

$$\dot{\alpha}_1^\varepsilon = (\varepsilon - i \operatorname{Im} \lambda_1) \alpha_1^\varepsilon + \frac{\int_{\mathcal{R}} u_1^* \mathcal{N}(\alpha_1^\varepsilon u_1 + \alpha_2^\varepsilon u_2)}{\int_{\mathcal{R}} u_1^* u_1}, \quad (3.18)$$

$$\dot{\alpha}_2^\varepsilon = (\varepsilon + i \operatorname{Im} \lambda_1) \alpha_2^\varepsilon + \frac{\int_{\mathcal{R}} u_2^* \mathcal{N}(\alpha_1^\varepsilon u_1 + \alpha_2^\varepsilon u_2)}{\int_{\mathcal{R}} u_2^* u_2}. \quad (3.19)$$

In order to argue that (3.18)-(3.19) exhibits a Hopf bifurcation to a periodic state, we now restrict the flow to the PT symmetric portion of the center subspace, and hence, in light of item (ii) above, to the PT symmetric subset of the center manifold. This amounts to the restriction $\alpha_2^\varepsilon = (\alpha_1^\varepsilon)^*$ and allows us to only work with (3.18). At this juncture, we make a change of variables of the form

$$a^\varepsilon := \alpha_1^\varepsilon + c_1 (\alpha_1^\varepsilon)^3 + c_2 |\alpha_1^\varepsilon|^2 (\alpha_1^\varepsilon)^* + c_3 ((\alpha_1^\varepsilon)^*)^3,$$

in order to convert the problem to its normal form, cf. [10], chapter 3. Writing the cubic nonlinear term in (3.18) as

$$n_1 (\alpha_1^\varepsilon)^3 + n_2 |\alpha_1^\varepsilon|^2 (\alpha_1^\varepsilon)^* + n_3 ((\alpha_1^\varepsilon)^*)^3 + n_4 |\alpha_1^\varepsilon|^2 \alpha_1^\varepsilon,$$

a tedious but direct calculation yields that with the choices $c_1 = \frac{n_1}{2 \operatorname{Im} \lambda_1} i$, $c_2 = -\frac{n_2}{2 \operatorname{Im} \lambda_1} i$, and $c_3 = -\frac{n_3}{4 \operatorname{Im} \lambda_1} i$, the new variable a^ε satisfies the simpler differential equation

$$\dot{a}^\varepsilon = (\varepsilon - i \operatorname{Im} \lambda_1) a^\varepsilon + n_4 |a^\varepsilon|^2 a^\varepsilon, \quad (3.20)$$

with the coefficient n_4 given by

$$n_4 = \frac{-\int_{\mathcal{R}} (|u_1|^2 u_1 u_1^* + 2 |u_2|^2 u_1 u_1^*) - i \int_{\mathcal{R}} ((\phi_{11} + \phi_{22}) u_1 u_1^* + \phi_{12} u_1^* u_2)}{\int_{\mathcal{R}} u_1 u_1^*}. \quad (3.21)$$

Here we have introduced the notation ϕ_{ij} to denote the solution to the equation

$$\Delta \phi_{ij} = \nabla \cdot \left(\frac{i}{2} [u_i \nabla u_j^* - u_j^* \nabla u_i] - u_i^* u_j h A_0 \right) = 0 \quad \text{for } i, j = 1, 2$$

subject to homogeneous Neumann boundary conditions on $\partial \mathcal{R}$ and zero mean on \mathcal{R} , so that $\tilde{\phi}(a^\varepsilon u_1 + (a^\varepsilon)^* u_2)$ in the nonlocal contribution \mathcal{N}_2 to the nonlinearity \mathcal{N} takes the form $|a^\varepsilon|^2 (\phi_{11} + \phi_{22}) + (a^\varepsilon)^2 \phi_{21} + ((a^\varepsilon)^*)^2 \phi_{12}$.

Provided $\operatorname{Re} n_4 < 0$, it is then easy to check from (3.20) that the system undergoes a supercritical Hopf bifurcation to a periodic solution given by

$$a^\varepsilon(t) = \frac{\varepsilon^{1/2}}{|\operatorname{Re} n_4|} e^{-i(\operatorname{Im} \lambda_1 + \gamma \varepsilon)t} \quad \text{where } \gamma := \frac{\operatorname{Im} n_4}{\operatorname{Re} n_4}. \quad (3.22)$$

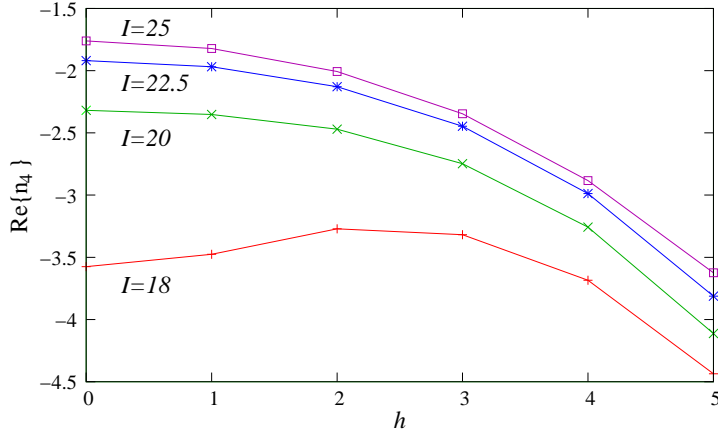


Figure 4: Graph showing the required negativity of the quantity $\text{Re } n_4$ as a function of h for various values of I . Here we have taken $L = 1$, $K = 2/3$ and $\delta = 4/15$. Other geometries were verified as well.

We have verified the condition $\text{Re } n_4 < 0$ numerically for a wide range of parameter values. See Figure 4.

Summarizing the analysis above, we have shown:

Theorem 3.2. *Fix a choice of parameters K, L, δ, h and I such that the first eigenvalue of \mathcal{L} in (3.4) satisfies $\text{Im } \lambda_1 \neq 0$ and n_4 given by (3.21) satisfies $\text{Re } n_4 < 0$. Then taking $\Gamma = \text{Re } \lambda_1 + \varepsilon$ in (2.1), there exists a value $\varepsilon_0 > 0$ such that for all positive $\varepsilon < \varepsilon_0$, the system (2.1)-(2.7) undergoes a supercritical Hopf bifurcation to a periodic state $(\psi_\varepsilon, \phi_\varepsilon)$. Applying (3.16) to this solution, we see that*

$$\left\| \psi_\varepsilon - \left(a^\varepsilon(t)u_1 + a^\varepsilon(t)^*u_1^\dagger \right) \right\|_{H^2(\mathcal{R})} \leq C\varepsilon^{3/2} \quad (3.23)$$

with a^ε given by (3.22).

Remark 3.3. *Though we do not present the analysis here, one can show that in fact this periodic solution is asymptotically attracting. Since there is no unstable subspace associated with \mathcal{L}_1 , nearby points off of the center manifold \mathcal{M}_ε are exponentially attracted to \mathcal{M}_ε . Then one argues that nearby non-PT symmetric points on \mathcal{M}_ε are attracted exponentially to the PT symmetric part of \mathcal{M}_ε . This type of argument was carried out in [22] and no doubt the same type of argument will work here though we have not checked the details.*

Remark 3.4. *One can also carry out the bifurcation analysis in the regime where λ_1 is real, which in particular would correspond to parameter regimes where I is sufficiently small. As our primary goal in this article is to address issues related to periodic phenomena raised in [3], [5] and [6] we did not pursue it here. In this case the center subspace*

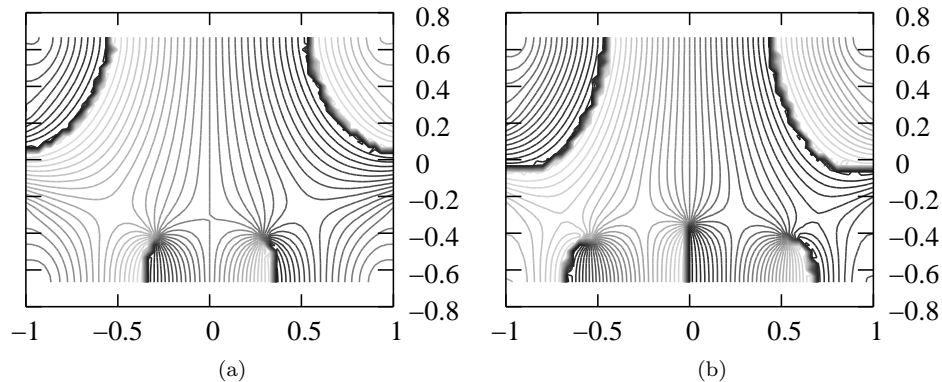


Figure 5: Stationary magnetic vortices. The curves represent level sets of the phase of the first eigenfunction u_1 . The geometry is $L = 1, K = 2/3, \delta = 4/15$. In (a) we used $h = 15$, while in (b) we used $h = 17$. In both cases we took $I = 10$ which is below the critical value I_c , so that a stationary vortex solution emerges to the full problem (2.1)-(2.7) with leading profile given by u_1 , cf. Remark 3.4

is simply spanned by u_1 and a stable stationary state emerges for $\varepsilon > 0$ of the form

$$\psi_\varepsilon \sim C\varepsilon^{1/2}u_1 \quad (3.24)$$

for some computable constant C . In the case where h is positive and sufficiently large, while λ_1 is real, one expects this stationary state to have magnetic vortices. Such a result might be compared to the single vortex stationary solution found in [9] for a similar model.

4 Vortex formation

As we mentioned in the Introduction, vortices form in this problem due to two separate effects. One type of vortex, that we term a magnetic vortex, is well-known. Magnetic vortices form as a result of the applied magnetic field, and can appear even when $I = 0$. We present two examples of such vortices in Figure 5. In both cases we used a rectangle with parameters $L = 1, K = 2/3, \delta = 4/15$. In Figure 5a the applied field is $h = 15$, while in Figure 5b the applied field is $h = 17$. In both figures the current is $I = 10$ which is below the critical current I_c for this geometry and these values of h . Hence, the first eigenvalue of the linearized problem is real and so the center manifold here is one-dimensional. This is the regime discussed in Remark 3.4. There are other examples, not shown, where vortices form even when $I = 0$.

What makes the present problem unusual is the formation of *kinematic* vortices, that is, vortices that are created even in the absence of magnetic fields. Physically, these vortices, just as the magnetic vortices, are points in space-time where the order parameter vanishes, the order parameter has a nonzero degree around these points, and large phase gradients occur near them. The formation of such kinematic vortices was extensively studied by Bendiyorov et al. [6] using numerical simulations of the TDGL

equations. The authors report on an unusual effect, where vortices appear periodically in pairs along the center line $x = 0$ of the rectangle, and move along it. They also found that, depending on the parameter values in the problem, vortices can either form at opposite sides of the boundary and annihilate inside or else nucleate together at an internal point on the center line and move away from each other towards the boundary. When $h = 0$, both vortices appear at the same time and they vanish, either by crossing the boundary simultaneously, or by annihilating each other, symmetrically about the line $y = 0$. When $h \neq 0$ the y -symmetry is broken: the creation of these kinematic vortices can take place at different times, and their motion is not symmetric with respect to the line $y = 0$.

We will use the theory developed in the preceding section to give a simple explanation for the formation and motion of kinematic vortices. Our analysis also gives a simpler means to compute when and where they form. In fact, we derive an explicit equation of motion for the kinematic vortices, fully based on the leading eigenfunction of the operator \mathcal{L} defined in equation (3.4). After deriving the equation of motion below, we demonstrate the different types of vortex creation and motion. One benefit of the new theory is that it allows us to easily detect additional types of kinematic vortex patterns, not observed in [6].

Mathematically, the formation and motion of the kinematic vortices are a consequence of the PT-symmetry of the problem. To see how they are created and move about, we consider the leading order term in the center manifold (cf. (3.23)):

$$\psi = a^\varepsilon(t)u_1 + a^\varepsilon(t)^*u_1^\dagger.$$

It is convenient to introduce the notation

$$a^\varepsilon = \xi \varepsilon^{-i\chi t}, \quad u_1(0, y) = g(y)e^{i\beta(y)},$$

where ξ and χ take the values provided in equation (3.22). Therefore, along the rectangle's central line the order parameter is given (at leading order) by

$$\psi(0, y, t) = 2\xi g(y) \cos(-\chi t + \beta(y)). \quad (4.1)$$

Hence, the order parameter vanishes on the central line $x = 0$ whenever the equation

$$\chi t = \beta(y) + \pi/2 + n\pi, \quad n = 0, \pm 1, \pm 2, \dots \quad (4.2)$$

holds. Equation (4.2) is the equation of both motion *and* creation of kinematic vortices.

Remark 4.1. *In the computation performed in this section we replaced the normalization condition (3.6) with the normalization $u_1(0, 0) = 1$. This condition has the advantage that for all parameters we have $\beta(0) = 0$, and therefore it is graphically easy to compare different β functions.*

The boundary conditions on u_1 imply $\beta'(\pm K) = 0$. Therefore, three simple shapes for β might be expected: upward hump, downward hump, or a monotone shape. However, our numerical study shows that, while indeed each of these shapes can occur, depending on the problem's parameters, other shapes are also present. Also, when $h = 0$, the

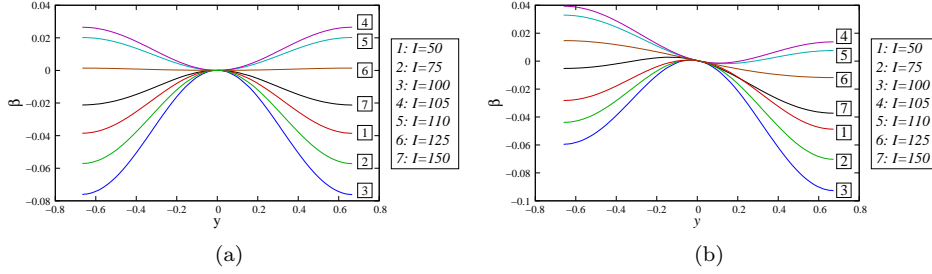


Figure 6: Different shapes for the function $\beta(y)$. The geometry is $L = 1, K = 2/3, \delta = 4/15$. In (a) we set $h = 0$, while in (b) we set $h = 0.05$.

problem is symmetric with respect to the y axis, and therefore β is either an even function, as in Figure 6a, or an odd function, if it is monotone. On the other hand, when the magnetic field is turned on, and $h \neq 0$, the symmetry of β is broken.

To demonstrate some of the different possible shapes of $\beta(y)$ and their dependence on the parameters in the problem, we refer to Figure 6. In all parts of this figure we took $L = 1, K = 2/3, \delta = 4/15$. In Figure 6a we set $h = 0$. Here β appears as an even function of y . Note that it changes its concavity depending on the values of the given current I . In Figure 6b we observe symmetry breaking in the shape of β under the influence of a nonzero applied field $h = 0.05$. In particular we point out that for some I levels the function $\beta(y)$ becomes a monotone function. We are still pursuing an explanation for the dramatic change in β as I varies from 100 to 105.

We now analyze four examples to illustrate the effect of the shape of the function β on vortex creation and motion.

Case 1: We refer to Figure 7. We use the same geometric parameters as before, namely, $L = 1, K = 2/3, \delta = 4/15$. We also use $I = 25, h = 0.05$. The function β is an asymmetric downward hump, as depicted in Figure 7a. The first solution of equation (4.2) occurs when t is large enough so that χt reaches $\beta(K) + \pi/2$ and a vortex emerges from the boundary. Then, as t increases the solution moves to lower values of y . When t is sufficiently large so that $\chi t = \beta(-K) + \pi/2$, a second vortex forms at the lower end $y = K$. As t grows further, both vortices move towards each other. When t reaches the level where $\chi t = \beta(y_m) + \pi/2$, where y_m is the location of the maximal point of β , the vortices collide and they annihilate. This is an example of annihilation of a vortex/anti-vortex pair, where we use ‘anti-vortex’ to refer to a vortex of negative degree. Then, there is a time interval where equation (4.2) does not hold for any y , and therefore there are no kinematic vortices at those times. This scenario repeats itself when $\chi t = \beta(-K) + 3\pi/2$ and so on. The creation, motion and annihilation of vortices are shown in Figure 7b for a half of a single period.

Case 2: Using the same parameters as in the previous example, except increasing the current I to take the value $I = 110$, gives rise to a different shape for $\beta(y)$. As depicted in Figure 8a, it is now a distorted U shape. Therefore, denoting the location of the minimum of β by y_m , when t reaches the value where $\chi t = \beta(y_m) + \pi/2$, a vortex/anti-vortex pair

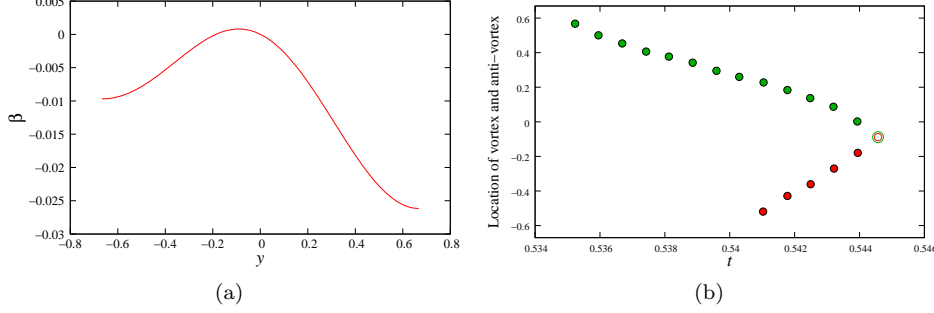


Figure 7: Creation and motion of kinematic vortices. (a) The function $\beta(y)$ for the parameters $L = 1, K = 2/3, \delta = 4/15, h = 0.05, I = 25$. (b) The circles describe the location of the vortices in the (y, t) plane.

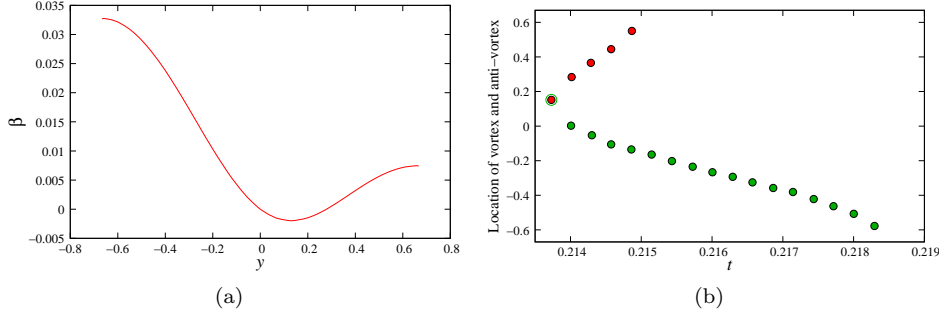


Figure 8: Creation and motion of kinematic vortices. (a) The function $\beta(y)$ for the parameters $L = 1, K = 2/3, \delta = 4/15, h = 0.05, I = 110$. (b) The circles describe the location of the vortices in the (y, t) plane.

is created inside the sample. As t increases, equation (4.2) is satisfied at two locations, until a point of time where $\chi t = \beta(K) + \pi/2$. After that, only one vortex remains in the rectangle, and this vortex eventually leaves the domain when $\chi t = \beta(-K) + \pi/2$. The motion of these kinematic vortices is depicted in Figure 8b.

Case 3: For the third example we maintain the same parameters as in the second example above, except that we increase h to take the value $h = 0.2$. For this choice of parameters $\beta(y)$ is a monotone function as depicted in Figure 9a. Now, the vortex is first created when $\chi t = \beta(K) + \pi/2$. It then travels to the lower end of the center line until $\chi t = \beta(-K) + \pi/2$. This motion is depicted in Figure 9b.

Case 4: In the fourth example we present a case where $\beta(y)$ has both a local maximum and a local minimum. The function $\beta(y)$ for the parameters $h = 20, I = 25$ is shown in Figure 10a. This is the parameter choice of Figure 3 as well. The geometry is the same as in the preceding examples. Following the scenarios above, if we look along the center line $x = 0$ we expect to see a first vortex emerging at $y = K$ at a time that we denote t_1 . Then, after this first vortex appears, a pair of vortices (of the same degree) appear

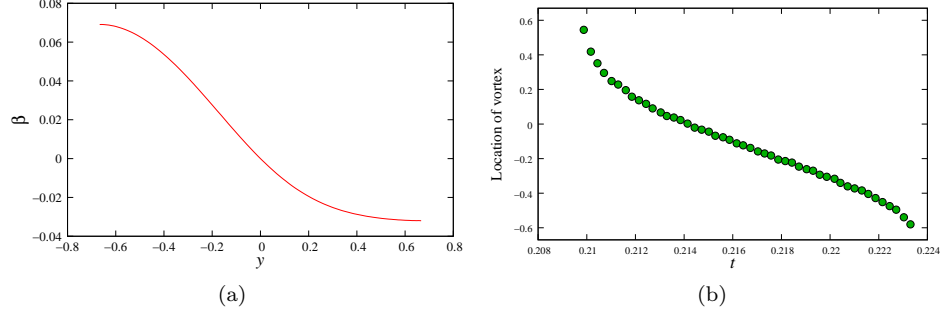


Figure 9: Creation and motion of kinematic vortices. (a) The function $\beta(y)$ for the parameters $L = 1, K = 2/3, \delta = 4/15, h = 0.2, I = 110$. (b) The circles describe the location of the vortices along the central line $x = 0$ in the (y, t) plane.

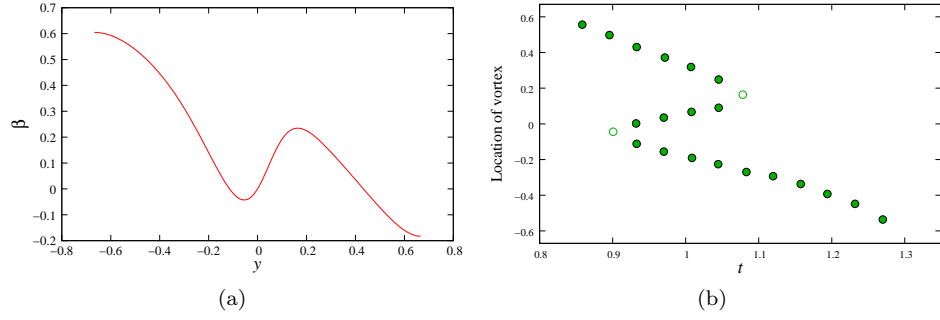


Figure 10: Creation and motion of kinematic vortices. (a) The function $\beta(y)$ for the parameters $L = 1, K = 2/3, \delta = 4/15, h = 20, I = 25$. (b) The circles describe the location of the vortices in the (y, t) plane.

at a later time, say t_2 , where $\chi t_2 = \beta(\bar{y}) + \pi/2$ and \bar{y} is the location of the interior local minimum of β . They move away from each other, until the one moving upward collides at a time t_3 with the first vortex moving downward. Finally, the remaining vortex that moves downward reaches the boundary $y = -K$ and exits the rectangle. This vortex creation and motion is indeed verified in Figure 10b.

This example, however, has several peculiar features. In Cases 1 and 2 vortices formed or disappeared in pairs of vortex-antivortex structure on the center line. In Case 4, on the other hand, the picture is different. We refer to a sequence of snapshots in Figure 11. In Figure 11a we observe five vortices, with only one on the center line. The two vortices far from the center line barely move throughout the period of the evolution. We view these two “sluggish” vortices as magnetic vortices. The vortex *on* the center line is the kinematic vortex that formed at $y = K$ at $t = t_1$ as explained above. The two vortices located on either side of the center line, and near it, which are of the same degree, move towards each other. Eventually they meet at $t = t_2$ on the center line, giving rise to the two kinematic vortices that were discussed above, and are shown in Figure 10b as well as Figure 11b. These two vortices move as described above until $t = t_3$. Then, the middle vortex on the center line meets the upper vortex on the center line. This is shown also in Figure 11c. Then, as shown in Figure 11d, this pair of vortices split away from the center line. This new pair of vortices moves away from the center line and upward, and the entire process repeats itself periodically.

The picture we just outlined indicates that kinematic vortices can move away from the center line. We therefore also term such vortices kinematic, namely those that spend part of a period on and part of a period off the center line, since their formation and motion follow directly from the PT symmetry and the structure it imposes on the center manifold.

5 Discussion

All of the examples from the previous section illustrate that, at least near the normal state, there is a dichotomy in vortex behavior when both applied currents and applied magnetic fields are present. The expansion based on center manifold reduction gives a partial explanation for this phenomenon, with the kinematic vortices arising in part due to the PT symmetry of the problem. In any event, it is clear that the variety of possible vortex behavior in this system is far more extensive than that seen in models capturing only magnetic effects. In particular, the motion law (4.2), based on small amplitude asymptotics rather than large Ginzburg-Landau parameter asymptotics as is more common in the literature, allows for a wide range of effects including boundary and interior nucleation, collision of like-signed vortices and periodicity of these events. Of course, all of the rigorous analysis we conduct necessarily involves small amplitude solutions since it is based on a bifurcation from the normal state. One would imagine that an even richer array of vortex behavior is possible for this system if one looks far from the normal state though an analytical approach would clearly require different tools.

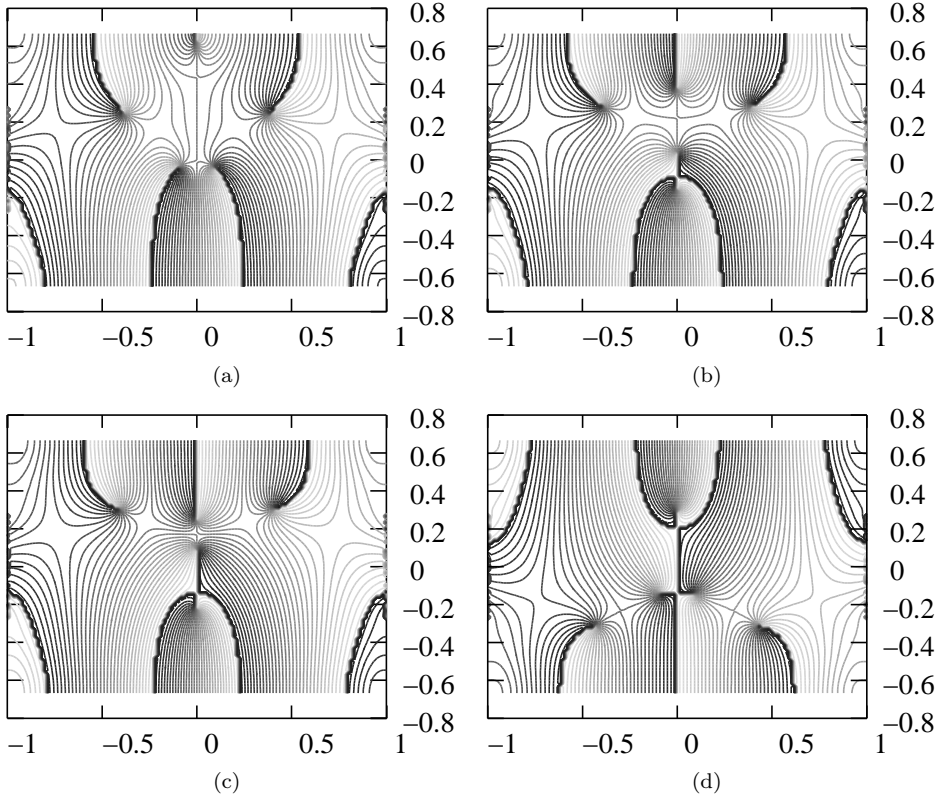


Figure 11: Contour plots of the phase of the order parameter for the parameters of Case 4 at four distinct times during a period of the motion. In (a) we see five vortices, one of them at the upper end of the center line. In (b) two vortices that were earlier off the center line move into it and meet there. Then they separate and start moving away from each other along the center line in (c), with the upper one moving upward to approach a south-moving vortex along the center line. In (d) these two vortices seem to collide and then veer away from each other. In these figures, the darkest lines are not significant in that they only represent a $-\pi$ to π jump in the phase. The tips of these lines, however, represent the vortices.

Acknowledgments. L. Peres Hari and J. Rubinstein were generously supported by an ISF grant. P. Sternberg was generously supported by NSF grant DMS-1101290 and a Simons Foundation Collaboration Grant.

References

- [1] Y. Almog, “The stability of the normal state of superconductors in the presence of electric currents,” *SIAM J. Math. Anal.*, **40**, no. 2, 824-850,(2008).
- [2] Y. Almog, B. Helffer and X. Pan, “Superconductivity near the normal state under the action of electric currents and induced magnetic fields in \mathbb{R}^2 ,” *Comm. Math. Phys.*, **300**, no. 1, 147-184, (2010).
- [3] A. Andronov, I. Gordion, V. Kurin, I. Nefedov and I. Shereshevsky, “Kinematic vortices and phase slip lines in the dynamics of the resistive state of narrow superconductive thin film channels,” *Physica C*, **213**, 193-199 (1993).
- [4] C.M. Bender and S. Boettcher, “Real spectra in non-Hermitian Hamiltonians having PT symmetry”, *Phys. Rev. Lett.* **80**, 5243 (1998).
- [5] G.R. Berdiyrov, A.K. Elmurodov, F.M. Peeters and D.Y. Vodolazov, “Finite-size effect on the resistive state in a mesoscopic type-II superconducting stripe,” *Phys. Rev. B*, **79**, 174506 (2009).
- [6] G.R. Berdiyrov, M.V. Milošević, F.M. Peeters and D.Y. Vodolazov, “Kinematic vortex-antivortex lines in strongly driven superconducting stripes,” *Phys. Rev. B*, **79**, 184506 (2009).
- [7] E. Caliceti, S. Graffi and J. Sjöstrand, “Spectra of PT-symmetric operators and perturbation theory,” *J. Phys. A.*, **38**, 185-193, (2005).
- [8] F. Cannata, J-P. Dedonder and A. Ventura, “Scattering in PT-symmetric quantum mechanics,” *Annals of Physics* **322**, no. 2, 397-433 (2007).
- [9] Q. Du, J. Wei and C. Zhao, “Vortex solution of the high κ , high field Ginzburg-Landau model with an applied current,” *SIAM J. Math. Anal.*, **42**, no. 6, 2368-2401, (2010).
- [10] M. Haragus and G. Iooss, “Local Bifurcations, Center Manifolds, and Normal Forms in Infinite Dimensional Dynamical Systems, Springer-Verlag, (2011).
- [11] D. Henry, “Geometric theory of semilinear parabolic equations,” *Lecture Notes in Mathematics*, vol. 840, Springer-Verlag, (1981).
- [12] B.I. Ivlev and N.B. Kopnin, “Electric currents and resistive states in thin superconductors,” *Adv. Phys.* **33**, 47-114 (1984).
- [13] L. Kramer and A. Baratoff, “Lossless and dissipative current carrying states in quasi one-dimensional superconductors,” *Phys. Rev. Lett.* **38**, no. 9, 518-521 (1977).

- [14] L. Kramer and R.J. Watts-Tobin, “Theory of dissipative current carrying states in superconducting filaments”, *Phys. Rev. Lett.* **40**, 1041 (1978).
- [15] J.E. Langer and V. Ambegaokar, “Intrinsic resistive transition in narrow superconducting channels”, *Phys. Rev.* **164**, 498 (1967).
- [16] H. Langer and C. Tretter, “A Krein space approach to PT-symmetry”, *Czechoslovak J. Phys.* **54**, 1113-1120 (2004).
- [17] T. Ma and S. Wang, *Phase Transition Dynamics*, Springer-Verlag, (2012).
- [18] S. Michotte, S. Mátéfi-Tempfli, L. Piraux, D.V. Vodolazov and F.M. Peeters, “Condition for the occurrence of phase slip centers in superconducting nanowires under applied current or voltage,” *Phys. Rev. B*, **69**, 094512, (2004).
- [19] K.G. Makris, R. El-Ganaini, D.N. Christodolous and Z. Musslimani, “Beam dynamics in PT symmetric optical lattices”, *Phys. Rev. Lett.*, **100**, 103904, (2008).
- [20] K.G. Makris, R. El-Ganaini, D.N. Christodolous and Z. Musslimani, “PT-symmetric periodic optical potentials”, *Int. J. Theor. Phys.*, **50**, 1019-1041, (2010).
- [21] J. Rubinstein, P. Sternberg and Q. Ma, “Bifurcation diagram and pattern formation in superconducting wires with electric currents,” *Phys. Rev. Lett.*, **99**, 167003, (2007).
- [22] J. Rubinstein, P. Sternberg and K. Zumbrun, “Resistive state in a superconducting wire: Bifurcation from the normal state,” *Arch. Rat. Mech. Anal.*, **195**, no. 1, 117-158 (2010).
- [23] S. Serfaty, I. Tice, “Ginzburg-Landau vortex dynamics with pinning and strong applied currents,” *Arch. Rat. Mech. Anal.*, **201**, no. 2, 413-464, (2011).
- [24] A.A. Shkalikov, “The limit behavior of the spectrum for large parameter value in a model problem”, *Math. Notes*, **62**, 796-799 (1997).
- [25] A.A. Shkalikov, “Spectral portraits of the Orr-Sommerfeld operator with large Reynolds numbers”, *J. Math. Sci.* **124**, 5417-5441 (2004).
- [26] I. Tice, “Ginzburg-Landau vortex dynamics driven by an applied boundary current,” *C.P.A.M.*, **63**, no. 1622-1676, (2010).
- [27] Wehrheim, K., *Uhlenbeck Compactness*, European Mathematical Society, (2004)